

ARMY RESEARCH LABORATORY



Response Characteristics of Active Scattering Aerosol Spectrometer Probes Made by Particle Measuring Systems

Ronald G. Pinnick, J. David Pendleton, and Gordon Videen

ARL-TR-1973

March 2000

20000502 127

Approved for public release; distribution unlimited.

The findings in this report are not to be construed as an official Department of the Army position unless so designated by other authorized documents.

Citation of manufacturer's or trade names does not constitute an official endorsement or approval of the use thereof.

Destroy this report when it is no longer needed. Do not return it to the originator.

Army Research Laboratory

Adelphi, MD 20783-1197

ARL-TR-1973

March 2000

Response Characteristics of Active Scattering Aerosol Spectrometer Probes Made by Particle Measuring Systems

Ronald G. Pinnick, J. David Pendleton, and Gordon Videen
Information Science and Technology Directorate

Approved for public release; distribution unlimited.

Abstract

Predictions are reported of the size response of various light-scattering aerosol counters manufactured by Particle Measuring Systems. Models considered are those that exploit the high intensity of light available within the cavity of a HeNe gas laser (generically referred to by the manufacturer as "active scattering aerosol spectrometer probes"). The new response function properly averages over particle trajectories through nodes, anti-nodes, and intermediate regions of the intracavity laser beam. Our studies address probes having two basic scattering geometries: those that collect light scattered over a relatively narrow solid angle (subtending angles between 4° and 22° from the laser beam axis) and those that collect light over a rather large solid angle (between 35° and 120°). The new response function predicts smoother dependence on particle size than the previous response function of Pinnick and Auvermann (1979, *J. Aerosol Sci.* **10**: 55-74) and is in better agreement with measurement. Response calculations for common atmospheric aerosol (water, sulfuric acid, ammonium sulfate, and black carbon) reveal the considerable sensitivity of the response to particle dielectric properties. Comparison of response calculations with the manufacturer's calibration reveals conditions for which the manufacturer's calibration is most appropriate, and the potential for errors (as much as a factor of two in sizing) when it is blindly applied. These results should help the user of these instruments to more realistically interpret size distribution measurements.

Contents

1	Introduction	1
2	Theoretical Response Function	5
3	Response Measurements	7
4	Response Predictions for Homogeneous Particles	11
5	Response Predictions for Inhomogeneous Particles	15
6	Comparison of New Response Function to PAG Theory	19
7	Predictions of Response for Multiline Laser Operation	23
8	Conclusion	25
	Appendices	27
A	Theoretical Response Function for Intracavity Laser Probes	27
	A-1 Intracavity Scattering	27
	A-2 Corrected PAG Response Function	32
	A-3 New Response Function	32
	A-4 Response Function for Multiline Lasing	34
B	Normalization of Measured Response to Theory	37
	Acknowledgments	39

References	41
Distribution	45
Report Documentation Page	47

Figures

1	Comparison of theoretical response and measured response for PMS narrow-angle scattering aerosol probes	8
2	Same as figure 1, except for PMS wide-angle scattering aerosol probes	9
3	Predicted response for PMS narrow-angle scattering probes	11
4	Same as figure 3, except for PMS wide-angle scattering probes and also Royco model 236	12
5	Relation between PMS-indicated particle radii and predicted particle radii for PMS ASASP-300 and ASASP-300X probes	13
6	Same as figure 5, except for PMS ASASP-X, ASASP-100X, LAS-X, LAS-250X, and HS-LAS probes	13
7	Predictions of response for PMS narrow-angle scattering probes to inhomogeneous particles	16
8	Same as figure 7, except for PMS wide-angle scattering probes and also Royco 236	18
9	Relation between PMS-indicated particle radii and predicted particle radii for narrow-angle scattering probes	20
10	Same as figure 9, except for PMS wide-angle scattering probes	21
11	Relation between PMS-indicated particle radii and predicted particle radii for wide-angle scattering probes	22
12	Predictions of response for PMS wide-angle scattering probes based on new response function	22
13	Predictions of response for PMS wide-angle scattering probes having lasers with sufficiently high gain for lasing in multiple lines	24

1. Introduction

Light-scattering particle counters are among the most widely used instruments for aerosol measurement. They have been employed for determining estimates of the tropospheric and stratospheric aerosol burden, for monitoring concentrations of particles in clean rooms essential for high-technology manufacturing, for determining aerosol filter efficiencies, for detecting atmospheric aerosol pollutants, for monitoring particulates in work place environments, etc.

These devices work as follows. Air containing particles is drawn through an illuminated volume, where light scattered by single particles is sensed and converted to an electrical signal whose pulse height is analyzed. The pulse height is used to infer particle size. The accumulated measurement of many particles results in a size distribution. Particle concentration is determined from total counts. Optical particle counters have the advantage of providing rapid, nonintrusive measurement of micrometer-sized aerosol particles, and can run continuously with only electrical power required for their operation.

About 25 years ago, Particle Measuring Systems (PMS) in Boulder, CO, began making several laser-based light-scattering particle counters (Schuster and Knollenberg, 1972; Knollenberg, 1976) for use by the aerosol community. During the late 1970s and early 1980s, a number of these instruments became available. The manufacturer refers to these counters as laser aerosol spectrometers, with the implication that they are superior to other light-scattering particle counters. In some of these instruments (the ASASP-300, ASASP-300X, ASASP-100X, ASASP-X, LAS-250X, LAS-X, HS-LAS, a number of aircraft versions of these probes, and various one-of-a-kind models), particles are illuminated by the intracavity light from a TEM₀₀ mode HeNe laser. The manufacturer generally designates these probes as "active cavity" (probes in which particles are illuminated outside the cavity are designated "passive cavity"). The active-cavity probes are the subject of this report.

There are basically two scattering geometries used in the active-cavity probes. In the ASASP-300 and ASASP-300X probes, the scattered light is collected by a lens over a relatively small and narrow solid angle subtending angles between 4° and 22° from the laser beam axis. In the more sensitive ASASP-X, ASASP-100X, LAS-250X, LAS-X, and HS-LAS probes,* scattered light is collected by a parabolic mirror, allowing collection over a relatively large and wide solid angle subtending angles between 35° and 120° from the laser beam axis. In both types of probes, the collection solid angle has symmetry about the laser beam axis. The "X" in the model designation denotes that the probe is plumbed with a relatively small inlet orifice (typically $200\ \mu\text{m}$ in diameter), so that all particles drawn through it intersect the illuminating laser. Because of the high intensity available within the cavity (more than 1 W intracavity circulating power for most models and up to 25 W for the high-sensitivity HS-LAS model), particles as small as $0.1\ \mu\text{m}$ in diameter can be measured.

However, even with their novel design and considerable sensitivity, these instruments are not without limitations: in particular, their size resolution, which we address in this report. Their sizing limitations arise from a fundamental fact: the light scattered by a particle depends on the particle's dielectric properties and shape as well as its size. Thus, unless particles of known refractive index are being measured, only an approximate determination of particle size can be made from the magnitude of its light-scattering signal.

Roughly 50 ASASP-300, 125 ASASP-X, 400 LAS-X, and 60 HS-LAS probes have been sold by PMS to date. Because of their wide use, the performance of these instruments has been studied rather extensively (Pinnick and Auverman, 1979; Pinnick and Rosen, 1979; Allan and Ashdown, 1982; Garvey and Pinnick, 1983; Solderholm and Salzman, 1984; Chen *et al.*, 1984; Liu *et al.*, 1985; Szymanski and Liu, 1986; Yamada *et al.*, 1986; Hinds and Kraske, 1986; Barnard and Harrison, 1988; Knollenberg, 1989; Jeung, 1990; Kim and Boatman, 1990; Pueschel *et al.*, 1990; Hering and McMurry, 1991; Liu *et al.*, 1992; Knollenberg and Veal, 1992; Kim, 1995).

Many of these studies concentrate on sizing performance where rather definitive measurements of response have been carried out on carefully prepared monodisperse aerosol test particles of different size, shape, and composition. Other studies have carried out theoretical investigations of particle response characteristics using the approximate response function

*Also the Royco 236 counter, for which the optical system was manufactured by PMS but sold in the early 1980s by Hiac-Royco, Menlo Park, CA.

proposed by Pinnick and Auvermann (1979) and Garvey and Pinnick (1983) (eq (2) of Pinnick and Auvermann, 1979, hereinafter referred to as the PAG response function).

For the narrow-angle scattering probes (ASASP-300 and ASASP-300X models), these studies reveal (1) a considerable sensitivity of the response to particle refractive index; (2) the existence of size regions where, because of Mie scattering resonances, particles of different size give the same response; and (3) degradation in size resolution for nonspherical particles because of the dependence of scattering on particle orientation. The same findings generally apply to the more commonly used wide-angle scattering probes (ASASP-X, ASASP-100X, LAS-X, LAS-250X, HS-LAS, and Royco 236 models). For both narrow-angle and wide-angle scattering probes, measurements of the response in the cited studies generally agree with the PAG response function, although the high-frequency oscillations predicted by the PAG response function were not found.

Although the PAG response function accounts for particle index of refraction, it is only approximate, because it does not account for particles traversing nodes, antinodes, and intermediate regions of the intracavity standing wave of the laser, nor does it account for laser mode changes during particle transit. Averaging over particle trajectories and phase smooths the response function and could result in better agreement with measurement.

For the LAS-X and the high-sensitivity HS-LAS probes, there may be additional smoothing caused by multiline lasing. In these probes, according to the manufacturer (Knollenberg, 1989), the laser used has sufficient gain to be above threshold for lasing in multiple lines. The PAG response function does not account for multiline lasing. Nor does it treat inhomogeneous particles.

We provide here an improved response function, which correctly averages over particle trajectory through the cavity of a laser and accounts for the laser coherence time being shorter than the time of transit of particles through the laser beam. This response function may have been suggested previously at a conference (Soderholm and Salzman, 1984), but there is insufficient information in the conference proceedings to judge. The new response function was suggested previously by Garvey and Pinnick (1983) (their eq (2)) but not recommended by them.

We compare the new response function, which is a smoother function of particle size than the PAG function, to previous response measurements of Pinnick and Auvermann (1979), Szymanski and Liu (1986), Garvey and

Pinnick (1983), and Chen *et al* (1984). The new response function is in better agreement with measurements of test aerosols compared to the PAG function. Thus, the measurements support the superiority of the new more general response function over the PAG response function.

Here we provide response calculations for both narrow-angle and wide-angle active-scattering probes, using the new response function, for both homogeneous and inhomogeneous particles characteristic of atmospheric and pollutant aerosol. For reference, we compare the results to the manufacturer's calibration, and to the previous PAG response function.

Finally, we present response calculations for a multiline laser source that may be used in the HS-LAS or LAS-X probes. Contrary to the manufacturer's claim, multiline operation has little effect on the probe response characteristics.

The results should enable users of these probes to better assess their sizing limitations.

2. Theoretical Response Function

Particles detected and sized in the active-cavity scattering probes are illuminated by the intracavity light from a TEM₀₀-mode HeNe laser. The particle cross section for light scattered into the probe collection aperture (defined as the probe response function R) should account for two averaging effects. First, because particles do not pass perpendicularly through the beam, they traverse nodes, antinodes, and intermediate regions (fringes) of the intracavity standing wave of the laser. Second, the coherence time of the laser is generally shorter than the particle transit time, causing the fringe positions to change during particle transit. In appendix A, we derive an expression for the response function that accounts for both of these effects. For spherical homogeneous particles, the result reduces to

$$R \simeq \frac{\pi}{k^2} \int_{\theta_{\min}}^{\theta_{\max}} \sin \theta \, d\theta \left[|S_1(\theta)|^2 + |S_2(\theta)|^2 + |S_1(\pi - \theta)|^2 + |S_2(\pi - \theta)|^2 \right], \quad (1)$$

where k is the wavenumber, θ is the scattering angle, and $S_1(\theta)$ and $S_2(\theta)$ are the amplitude scattering matrixes (Bohren and Huffman, 1983).

In appendix A we also derive a corrected expression for the PAG theory, which assumes that (1) the particle trajectory is perpendicular to the intracavity standing wave, (2) the particle passes through an antinode, and (3) the coherence time of the laser is longer than the particle transit time through the beam. The result is

$$R \simeq \frac{\pi}{k^2} \int_{\theta_{\min}}^{\theta_{\max}} \sin \theta \, d\theta \left[|S_1(\theta) + S_1(\pi - \theta)|^2 + |S_2(\theta) - S_2(\pi - \theta)|^2 \right]. \quad (2)$$

This response function is slightly different from the PAG response function:

$$R \simeq \frac{\pi}{k^2} \int_{\theta_{\min}}^{\theta_{\max}} \sin \theta \, d\theta \left[|S_1(\theta) + S_1(\pi - \theta)|^2 + |S_2(\theta) + S_2(\pi - \theta)|^2 \right]. \quad (3)$$

Finally, we address the issue of multiline lasing. Lasers in some of the active-cavity probes have high gain and lase on multiple lines. We show

in appendix A that for multiwavelength operation, the response function is a sum of the response functions at each wavelength weighted by the appropriate irradiance fraction in each wavelength.

3. Response Measurements

A definitive test of the validity of the theoretical response function (eq (1)) requires measurement of well-characterized monodisperse test particles having a range of sizes and refractive indexes. For active-cavity probes there is an abundance of measurements available. Here we concentrate on the measurements of Pinnick and Auvermann (1979) for the ASASP-300, Garvey and Pinnick (1983) for the ASASP-X, Chen *et al* (1984) for the Royco 236, and Syzmanski and Liu (1986) for the ASASP-300X and LAS-X.

We first consider the narrow-angle scattering probes (ASASP-300 and ASASP-300X). Figure 1 shows the measured response to nonabsorbing polystyrene latex and dioctylphthalate (DOP) particles and to highly absorbing nigrosin dye and carbon black particles, compared to the theoretical response function (eq (1)). For each probe, a single normalization constant relating response voltage to particle cross section is determined from a fit of the experimental data for polystyrene latex to the theoretical curve for latex. This fitting procedure is described in appendix B.

The measurements confirm the predicted oscillatory character of the response curve for nonabsorbing latex and DOP particles, although the fine structure cannot be resolved. The measurements also generally corroborate the smooth monotonic response predicted for highly absorbing particles. As noted previously by Pinnick and Auvermann (1979), the fall-off in the observed response for highly absorbing nigrosin particles for radii greater than $1 \mu\text{m}$ is believed to be due to a reduction of laser power caused by the particles. The disagreement between carbon black measurements and theory could result from the difficulty in preparing homogeneous spherical particles (having refractive index $1.775 - 0.508i$ as used in the theory) from India ink.

A similar comparison for several models of the wide-angle probes (the ASASP-X, LAS-X, and Royco 236) is shown in figure 2. Again, we emphasize that we determined a single normalization factor for each probe by doing a weighted fit of the polystyrene latex measurements to the theoretical response. The theoretical response is generally within the error of measurement, or what appear to be errors in measurement, as evidenced by

Figure 1. Comparison of theoretical response (eq (1)) and measured response for PMS narrow-angle scattering aerosol probes. Theory and measurements are shown for nonabsorbing polystyrene latex and dioctylphthalate, and highly absorbing nigrosin dye and carbon black. Data sets are offset by 1 to 3 orders of magnitude on vertical scale, as indicated. A single normalization factor for each probe relates experimental response voltage to particle-scattering cross section. Predicted broad Mie scattering resonance features are corroborated by measurements.

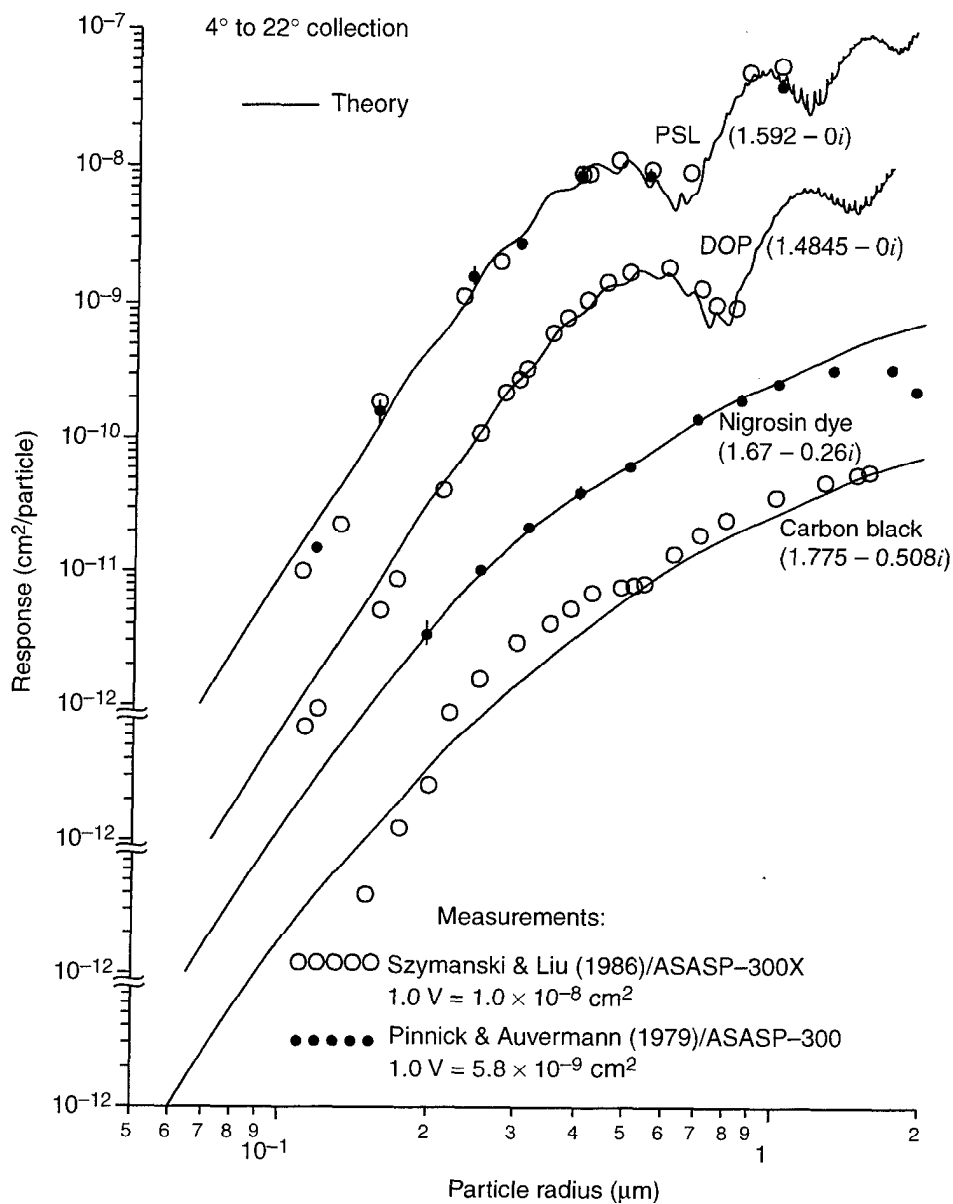
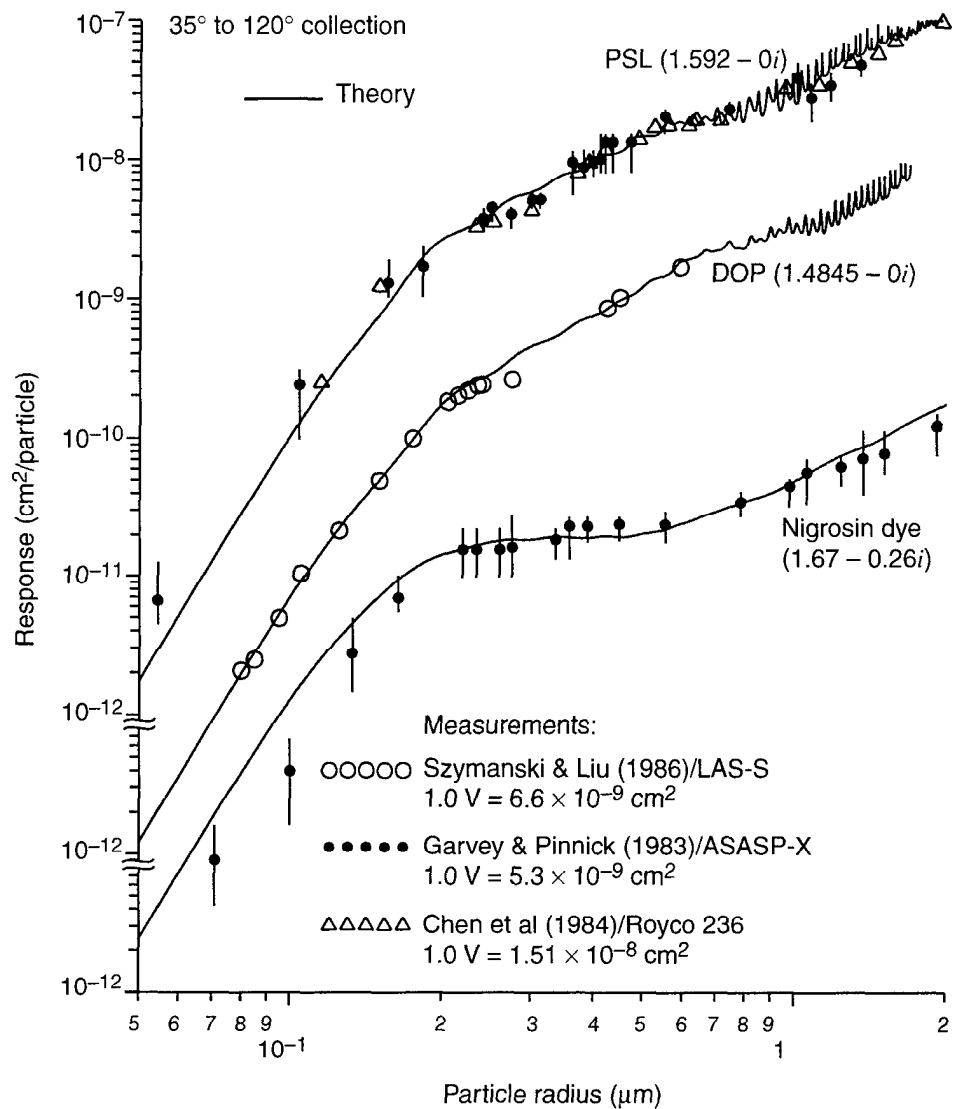


Figure 2. Same as figure 1, except for PMS wide-angle scattering aerosol probes. Predictions agree with measurements and reveal a generally monotonic increase of response with particle size for both nonabsorbing and absorbing particles.



fluctuations in the data points where no error bars are given, for both non-absorbing and absorbing particles. The theoretical curves and measured response data reveal an almost monotonic increase in response with increasing particle size, although the response increases slowly with increasing size for highly absorbing particles with $0.2 \mu\text{m} < r < 0.6 \mu\text{m}$.

Collectively, the comparison of measured response with the theoretical response for both narrow-angle and wide-angle scattering probes reveals

that (1) the response function (eq (1)) that properly averages over intracavity particle trajectories is in slightly better agreement with measurement compared to the previous PAG response function (eq (3)), and (2) the fine structure predicted by the response function (eq (1)) is not experimentally resolved.

This latter finding is not surprising, since the amplitude of the fine structure is of the order of the pulse height channel widths in these probes, and thus we should not expect them to be resolved. Even the use of a pulse height analyzer with greater resolution may not resolve the fine structure because of basic limitations of these instruments (laser intensity variations for different particle trajectories, etc).

We conclude that the theoretical response function (eq (1)) can adequately predict the response of both narrow-angle and wide-angle scattering probes to spherical particles, regardless of their dielectric properties, so long as they are of uniform composition. We provide such predictions for some common atmospheric aerosols in the next section.

4. Response Predictions for Homogeneous Particles

Atmospheric aerosols can be irregular and of mixed composition. However, some occur as spherical and homogeneous particles. We consider four types of aerosol particles that are common in the earth's atmosphere: water droplets, droplets composed of a 75-percent sulfuric acid/25-percent water mixture, ammonium sulfate particles, and particles of black carbon. In addition, for generality, we consider metal particles of copper. We initially assume all to be spherical and homogeneous. Figures 3 and 4 present response calculations for these aerosols for both narrow-angle and wide-angle scattering probes. For reference, these calculations are compared to the manufacturer's calibration, which is plotted on the particle-scattering cross-section scale after normalization by the factors determined in the previous section (from fitting the polystyrene latex measurements to theory).

Figure 3. Predicted response for PMS narrow-angle scattering probes (ASASP-300 and ASASP-300X). Curves for water, 75% sulfuric acid in water, ammonium sulfate, black carbon, and copper are shown. Response is a sensitive function of particle refractive index. Particles differing by a factor of two in radius can have same response. Manufacturer's calibration for a ASASP-300 probe is given for reference.

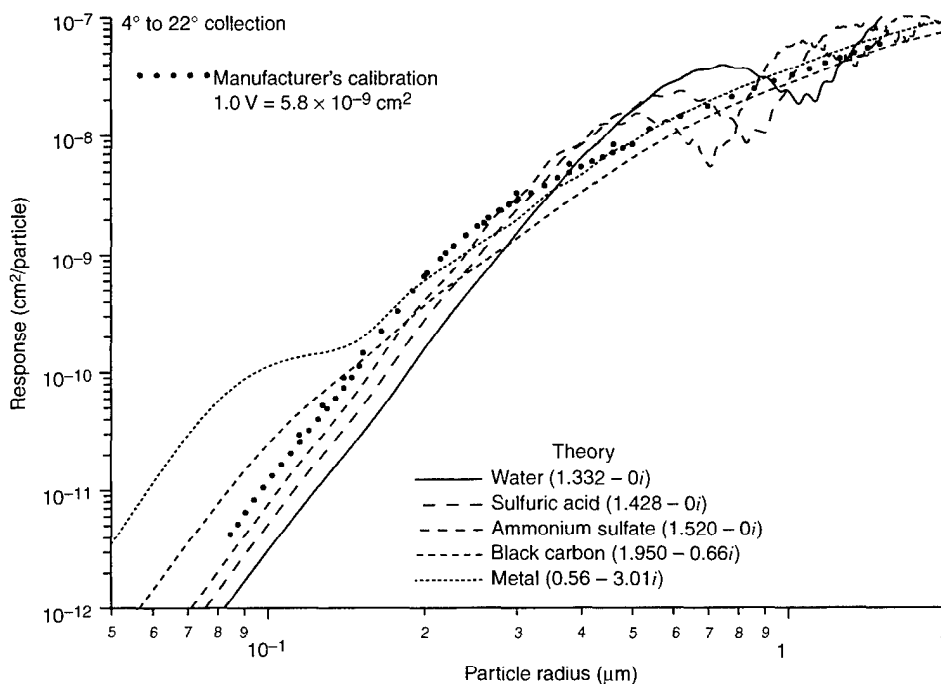
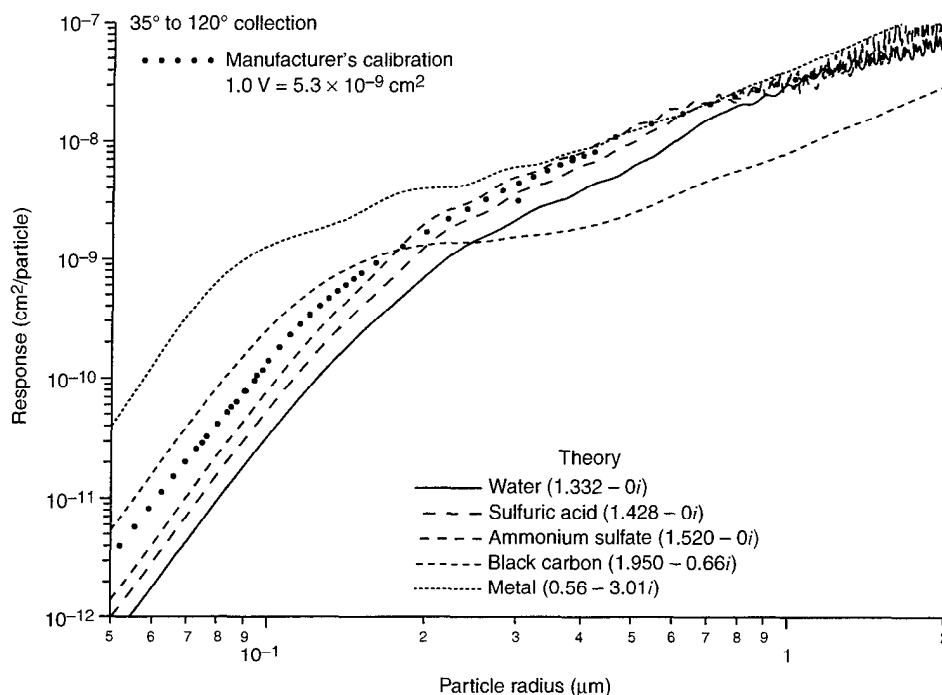


Figure 4. Same as figure 3, except for PMS wide-angle scattering probes (ASASP-X, ASASP-100X, LAS-X, LAS-250X, HS-LAS models) and also Royco model 236. As for narrow-angle scattering probes, particles differing by a factor of two in radius can have same response. Manufacturer's calibration is for an ASASP-X.



These results confirm what is already well known: the response for both types of probes depends on particle refractive index as well as size. Measurement of particles having a range of compositions (and refractive indexes) degrades the size resolution of the probes considerably, as particles of radii differing by as much as a factor of two can have the same response.

As is evident from the figures, the manufacturer's calibration passes through the family of curves that represent commonly occurring atmospheric aerosol constituents. Thus, for measurement of unknown aerosol that consists of particles of widely different composition (as for example in the earth's tropospheric mixed layer), the manufacturer's calibration, even though it divides size intervals into too many channels to be meaningful, might be appropriate for obtaining average size distributions.

If the manufacturer's calibration is used to infer particle size, the errors resulting from refractive index effects are more easily revealed in figures 5 and 6, where we plot the PMS (manufacturer's calibration) indicated radii versus the actual (theoretical response function) radii. For both probes, the PMS-indicated radius is generally in error by less than 50 percent. Note that for the narrow-angle scattering probes, the PMS-indicated radius can be multivalued.

Figure 5. Relation between PMS-indicated particle radii (smooth curve through manufacturer's calibration) and predicted particle radii (theoretical response function) for PMS ASASP-300 and ASASP-300X probes. Solid straight line is a reference depicting perfect agreement between indicated and predicted size. Curves for water, 75% sulfuric acid in water, ammonium sulfate, black carbon, and copper are shown. Errors in indicated radii are generally less than $\pm 50\%$.

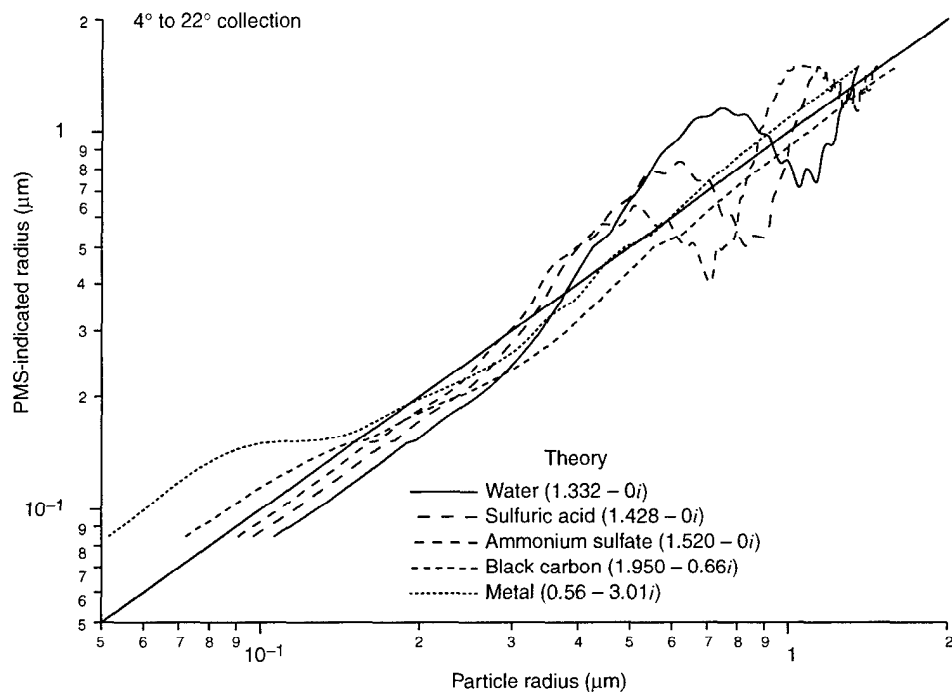
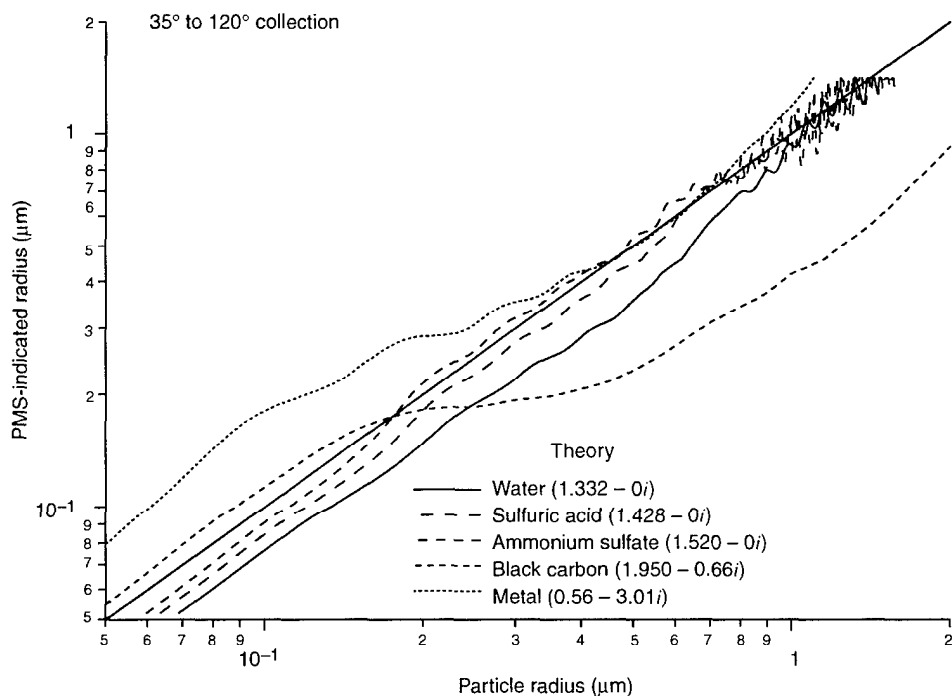


Figure 6. Same as figure 5, except for PMS ASASP-X, ASASP-100X, LAS-X, LAS-250X, and HS-LAS probes. Errors in PMS-indicated radii are generally less than $\pm 50\%$.



These results give a comprehensive assessment of the response of the PMS probes to homogeneous spherical particles, but what about aerosol particles that are inhomogeneous?

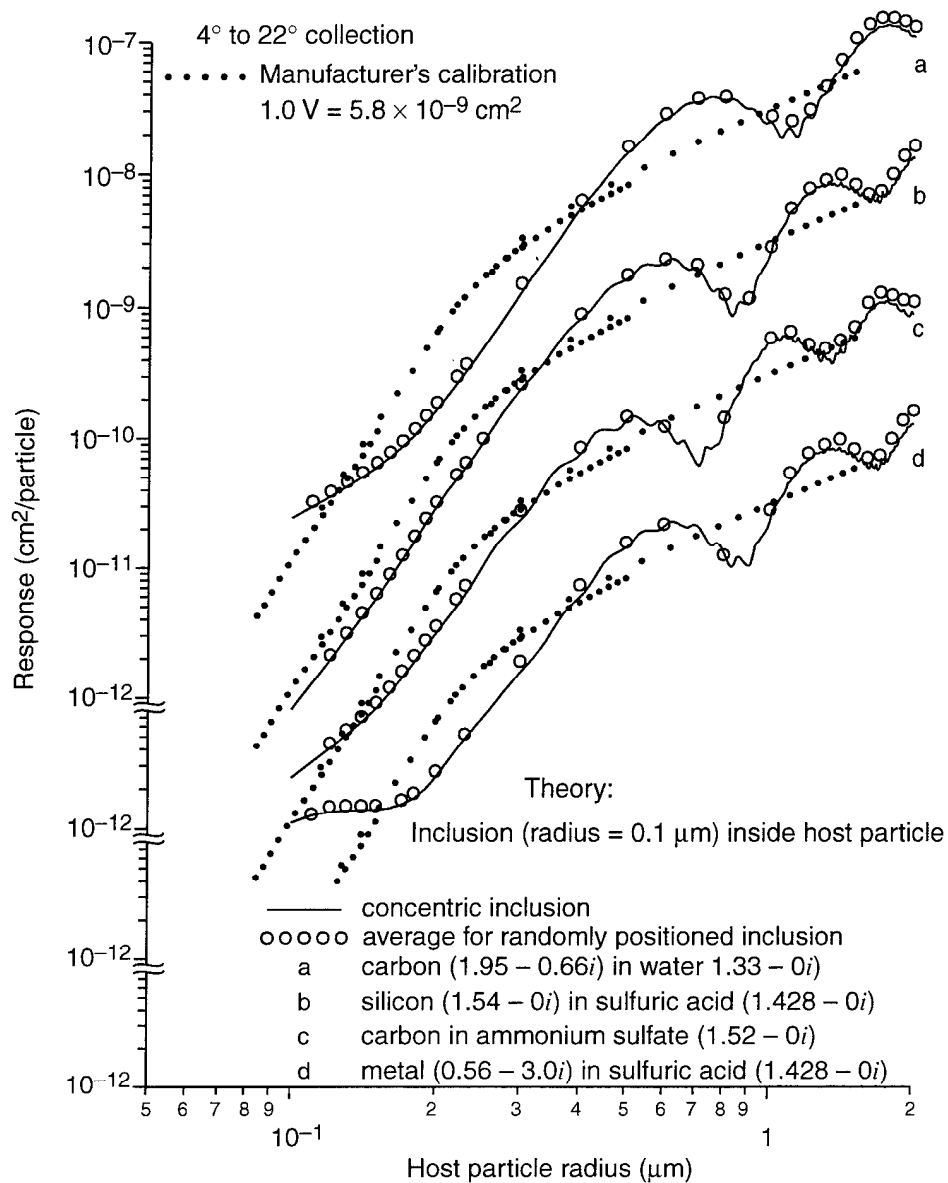
5. Response Predictions for Inhomogeneous Particles

For many applications, not only does the aerosol of interest consist of particles of different composition, but single particles may be composed of mixtures (black carbon in ammonium sulfate, black carbon in quartz, clay minerals in quartz, black carbon in water, sulfuric acid with crustal core, ammonium sulfate in sulfuric acid, silica shards in black carbon agglomerates, metals in sulfuric acid, etc). Such particles can have very complicated morphology (Gillette and Walker, 1977; Chylek *et al*, 1981; Pinnick *et al*, 1985; Sheridan and Musselman, 1985; Sheridan, 1989a, 1989b; Sheridan *et al*, 1993; Reitmeijer and Janeczek, 1997). To predict the response of the probes to internal mixtures, we modify the response function (eq (1)) by choosing the simplest possible model: that of a sphere containing a spherical inclusion (Ngo *et al*, 1996). We consider four specific particle types: a water droplet containing a black carbon inclusion, a sulfuric acid droplet containing quartz, an ammonium sulfate particle containing carbon, and a sulfuric acid droplet containing metal.

We consider the narrow-angle scattering probes first. To calculate the response function for black carbon in a water droplet sulfate host, we neglect the fractal cluster morphology of black carbon (Forrest and Witten, 1979; Colbeck *et al*, 1989) and assume a solid black carbon core or inclusion with fixed radius of $0.1 \mu\text{m}$ enclosed within the host. We calculate the response in two ways. First we assume the core is located in the center of the host particle and increase the host size. These results are displayed by the solid curves in figure 7. Then we relax this assumption and let the inclusion be randomly positioned within the particle, and calculate the response for each position. The larger the host particle, the more possible positions are considered. The average of these response values is shown by the corresponding open circles in figure 7. The standard deviations of the response values for different inclusion positions are also calculated but not displayed. Results are calculated for only a small number of host particle sizes because of the considerable computational requirements. For reference, the manufacturer's calibration is also shown.

For simplicity, in calculating the response for other internal mixtures, we fix the inclusion size to be the same as for black carbon in water (i.e., inclusion

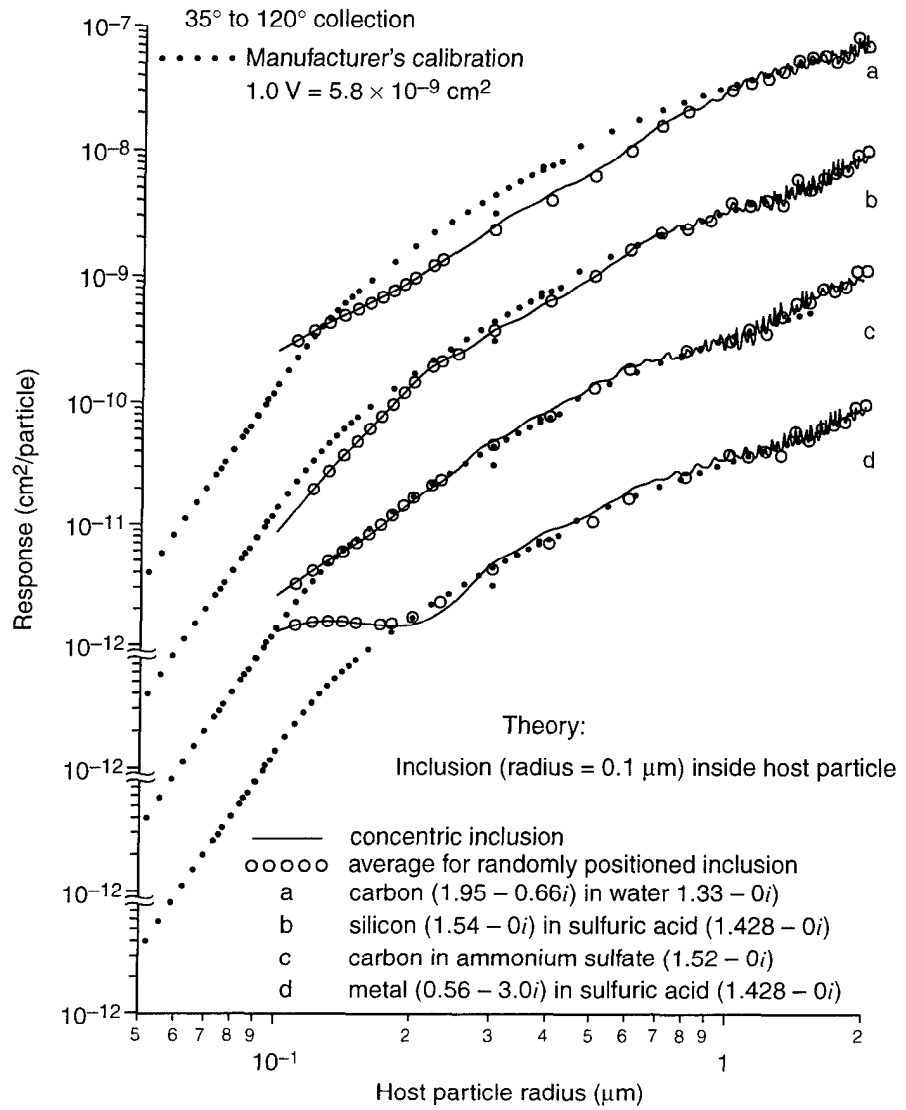
Figure 7. Predictions of response for PMS narrow-angle scattering probes (models ASASP-300 and ASASP-300X) to inhomogeneous particles: black carbon inclusions in water, quartz in sulfuric acid, black carbon in ammonium sulfate, and metal in sulfuric acid. Solid curves are for a 0.1- μm -radius inclusion at center of particle; open circles denote average response values for inclusion positioned randomly within particle. Data sets are offset by 1 to 3 orders of magnitude on vertical scale as indicated. Response of a composite particle rapidly transitions from that of inclusion (for composite particle radius near 0.1 μm) to that of host as host radius is increased. Manufacturer's calibration is shown by solid dots.



radius $r = 0.1 \mu\text{m}$). The response calculations for internal mixtures using this simple model of a sphere containing a spherical inclusion reveal the following: (1) for small host sizes, where the inclusion nearly fills the host, the response approximates that of the inclusion, but quickly transitions, as the host size increases, to a response approximating that of the host; (2) the average response for a randomly positioned inclusion is generally within 20 percent of the response for a concentric inclusion; (3) the variation in response due to changing orientation is small, as revealed by the standard deviations of the response for a randomly positioned inclusion generally being only about 10 percent of the average response; and (4) as for most homogeneous particles, the manufacturer's calibration is not a very good approximation of the predicted response, since the result in some size regions is undersizing, and in others oversizing.

Figure 8 presents the response of the wide-angle scattering probes to particles containing inclusions. Again, the average response for a randomly positioned inclusion is generally within 20 percent of the response for a concentric inclusion (detailed comparisons show that for carbon in water, the difference is less than 13 percent, for silicon in sulfuric acid 3 percent, for carbon in ammonium sulfate 10 percent, and for metal in sulfuric acid 22 percent). However, unlike for the narrow-angle scattering probes, the manufacturer's calibration is quite a good representation of the probe's response for some internal mixtures: quartz in sulfuric acid, black carbon in ammonium sulfate, and metal in sulfuric acid (so long as the sulfuric acid mass fraction dominates). The manufacturer's calibration is less valid for a mixture of black carbon in water.

Figure 8. Same as figure 7, except for PMS wide-angle scattering probes (ASASP-X, ASASP-100X, LAS-X, LAS-250X, HS-LAS models) and also Royco 236.



6. Comparison of New Response Function to PAG Theory

What are the differences between the results of using the new response function (which properly accounts for particle trajectory through nodes, antinodes, and intermediate regions of the intracavity laser beam) and the results of using the previously published PAG theory approximation (which assumes particle trajectories pass through only antinodes of the beam)? How do these response functions compare to the manufacturer's calibration? To address these questions, we have compared the response functions by making graphs of the PMS-indicated size (manufacturer's calibration) versus the actual size (predicted).

Results for particles that are nonabsorbing ($m = 1.50 - 0i$) and absorbing ($1.95 - 0.66i$) are displayed in figure 9 (for narrow-angle scattering probes) and figure 10 (wide-angle scattering probes). The difference between the new response function (eq (1)) and the PAG response function (eq (3)) results is small, particularly for highly absorbing particles. For nonabsorbing particles, the amplitude of the high-frequency oscillations is much reduced for the new response function compared to the PAG response function. For highly absorbing particles, the response functions for the narrow-angle scattering probes are indistinguishable. A similar comparison for the corrected PAG response function (eq (2)) in figure 11 reveals small differences from the original PAG response function (eq (3)).

Figure 12 presents a more direct comparison of the new response function and the PAG response function for the wide-angle scattering probes. For nonabsorbing particles with refractive index $m = 1.50 - 0i$, the new response function is a smoother function of particle size compared to the PAG response function.

Figure 9. Relation between PMS-indicated particle radii (smooth curve through manufacturer's calibration) and predicted particle radii (new response function and PAG response function) for narrow-angle scattering probes. Solid straight line is a reference depicting perfect agreement between indicated and predicted size. Curves for nonabsorbing and highly absorbing particles are shown. Difference between new response function and PAG response function results is small for both absorbing and nonabsorbing particles. Normalization in factor relating manufacturer calibration to theoretical response is $1 V = 5.8 \times 10^{-9} \text{ cm}^2$.

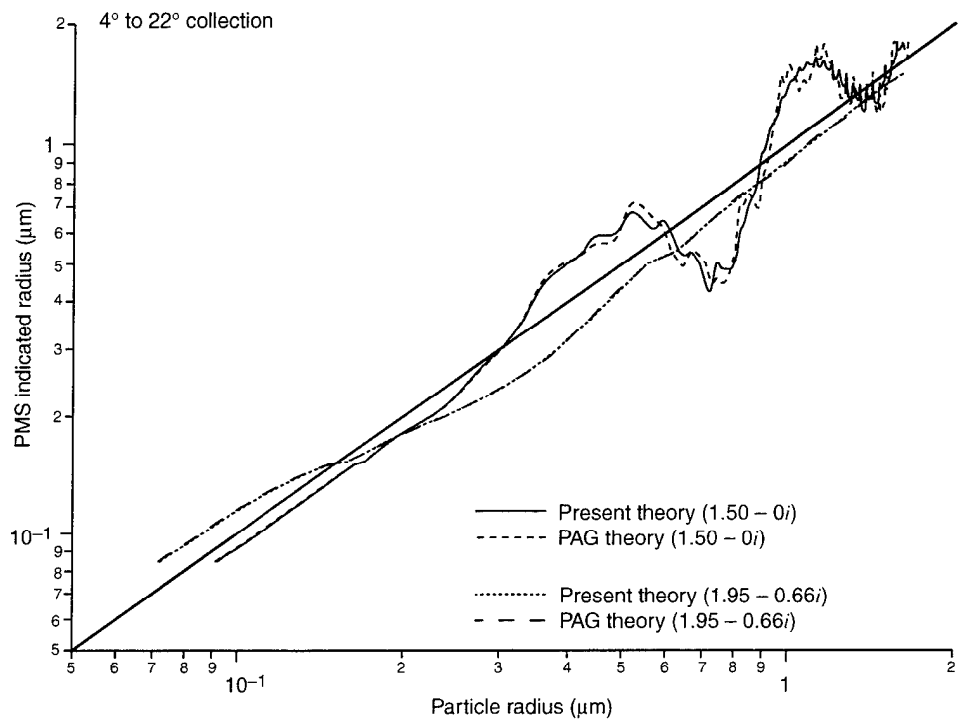


Figure 10. Same as figure 9, except for PMS wide-angle scattering probes. Large-amplitude oscillations in PAG response function are not evident in new response function.

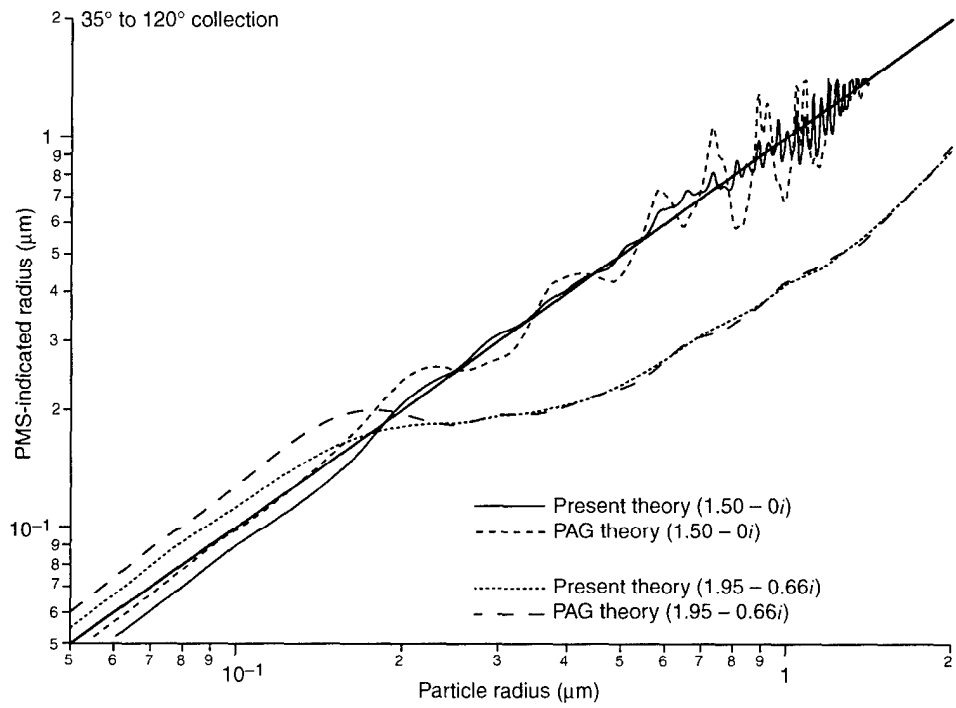


Figure 11. Relation between PMS-indicated particle radii (smooth curve through manufacturer's calibration) and predicted particle radii (corrected PAG response function, eq (2), and PAG function, eq (3)) for wide-angle scattering probes. Solid straight line is a reference depicting perfect agreement between indicated and predicted size. Curves for nonabsorbing and highly absorbing particles are shown. Normalization factor relating manufacturer calibration to theoretical response is $1 V = 5.3 \times 10^{-9} \text{ cm}^2$.

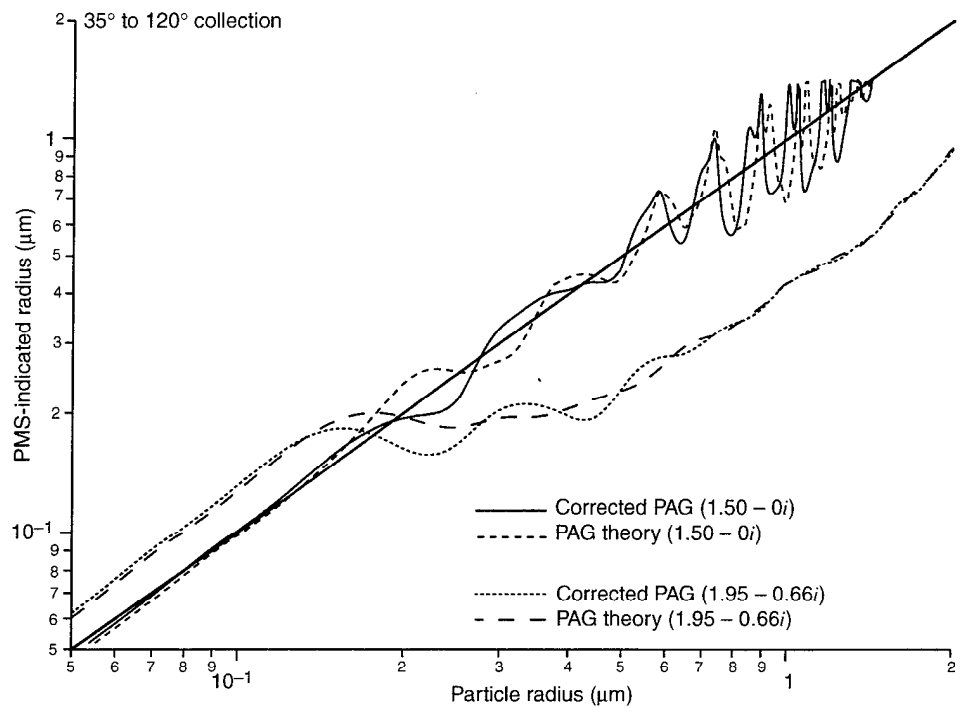
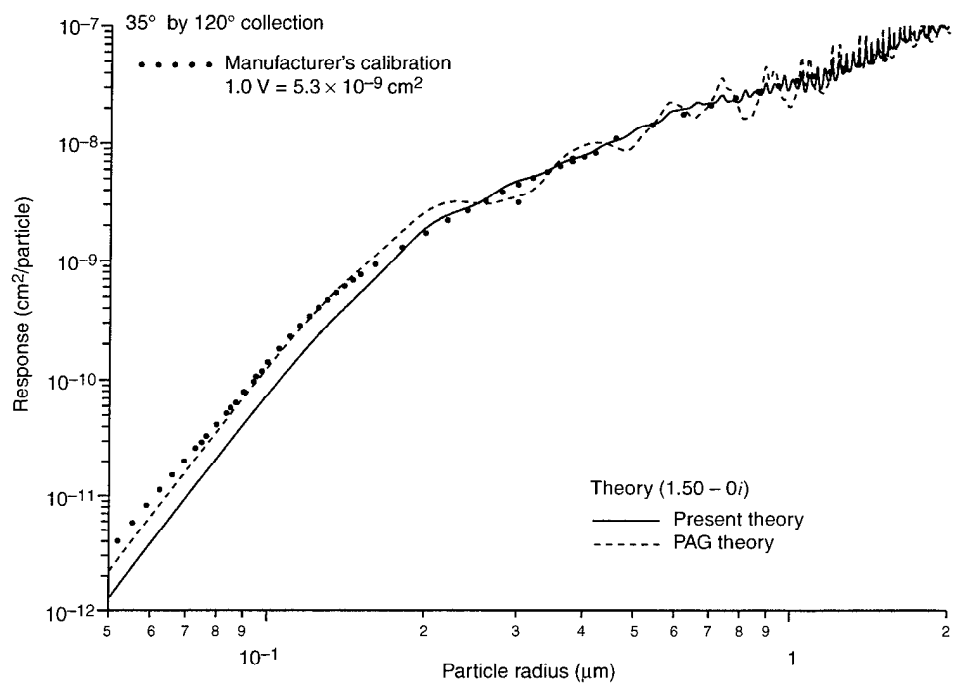


Figure 12. Predictions of response for PMS wide-angle scattering probes based on new response function (eq (1)) and PAG response function (eq (3)), compared to manufacturer's calibration. For particles with $m = 1.50 - 0i$, manufacturer's calibration follows PAG theory and undersizes particles with radii less than $0.2 \mu\text{m}$.



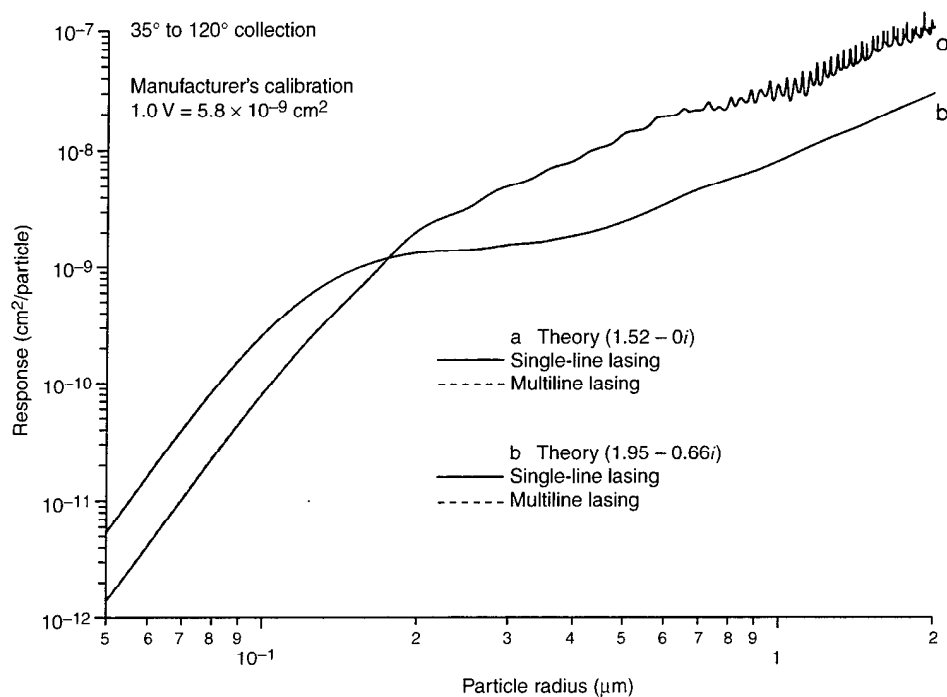
7. Predictions of Response for Multiline Laser Operation

The manufacturer claims (Knollenberg, 1989) that the HeNe lasers in the LAS-X and HS-LAS probes have sufficient gain to operate in multifrequency modes, with as many as six lines from yellow to red for the HS-LAS, and that the multifrequency operation smooths the response characteristics of the instrument. To address this claim, we consider particle scattering in a cavity lasing in multiple lines.

As shown in appendix A, one can calculate the response function for multiline operation by weighing the response function for each line by the intensity of that line (eq (A-27)). According to PMS, the intensity distribution for the HS-LAS is typically 80 percent for the 632.8-nm line, 10 percent for the 629.4-nm line, and 10 percent for all other lines (private communication, John Mitchell, Particle Measuring Systems, 1998). We note that by measuring the light transmitted through the highly reflecting closure mirror of a factory-refurbished LAS-X (serial number 9075-0786-252, manufactured in July 1986), we found 98-percent intensity in the 632.8-nm line, 2-percent intensity in the 640.1-nm line, and no measurable intensity in the other lines. Thus the manufacturer's claim of multiline operation may be exaggerated.

Nevertheless, lasers in the HS-LAS probes purportedly have higher gain than those in the LAS-X probes. To assess the effect of multiline operation, we assume the manufacturer's claim is correct and calculate the response of the HS-LAS (wide-angle scattering probe) for the following distribution of intensities: 80 percent at 632.8 nm, 10 percent at 629.4 nm, and 2 percent each at the 593.9-, 604.6-, 611.8-, 635.2-, and 640.1-nm lines. Figure 13 compares the results for multiline lasing and single-line lasing (all intensities at 632.8 nm). Response calculations are presented for nonabsorbing ammonium sulfate and highly absorbing black carbon. In both cases the difference in response cannot be distinguished in the figure (even though it may not be clearly evident, two curves are displayed for each refractive index). Numerical results show that the differences are less than 7 percent for ammonium sulfate and less than 2 percent for black carbon. Thus the effect of multiline lasing on response is negligible.

Figure 13. Predictions of response for PMS wide-angle scattering probes having lasers with sufficiently high gain for lasing in multiple lines (LAS-X, LAS-250X, HS-LAS models). Response curves are presented for multiline and single-line lasing operation. Curves are presented for nonabsorbing ammonium sulfate ($m = 1.52 - 0i$) and highly absorbing black carbon ($m = 1.95 - 0.66i$) particles (two curves are presented for each refractive index). Multiline operation has negligible effect on response characteristics.



8. Conclusion

We present here an improved response function for light-scattering aerosol counters that use intracavity laser illumination. The new response function predicts a smoother size dependence compared to the previous PAG response function, particularly for nonabsorbing particles, because it accounts for phase averaging. The response function has been used to investigate the response characteristics of Particle Measuring Systems aerosol probes that use intracavity laser illumination. Probes having two scattering geometries have been studied: those that collect light scattered through angles ranging from 4° to 22° from the direction of the laser-beam axis (as in ASASP-300 and ASASP-300X style probes), and those that collect light scattered 35° to 120° from the laser-beam axis (as in the ASASP-X, ASASP-100X, LAS-250X, LAS-X, and HS-LAS probes). The new response function is generally in good agreement with measurements on uniform particles of polystyrene latex, dioctylphthalate, nigrosin dye, and carbon black. Response calculations for both homogeneous and inhomogeneous particles with a variety of refractive indexes are presented and compared to the manufacturer's calibration; this comparison reveals that caution needs to be exercised in using the calibration. For the wide-angle scattering probes, our study suggests that the manufacturer's calibration is generally appropriate for sizing sulfate particles, as well as particles containing mixtures of black carbon in sulfate and quartz in sulfuric acid. Contrary to the manufacturer's claim, multiline laser operation has little effect on probe response characteristics.

Appendix A. Theoretical Response Function for Intracavity Laser Probes

A-1 Intracavity Scattering

In active-cavity scattering probes, aerosol particles traverse an intracavity laser beam within an optical cell. Scattered light is collected either by a lens (for the narrow-angle scattering probes) or by a parabolic mirror (for the wide-angle scattering probes). In both instruments, the collection solid angle is symmetric about the beam axis, except for small asymmetry caused by the aerosol entrance jet and exit port, which protrude into the optical cell in the X-probes. These ports reduce in a small but complicated fashion the solid angle over which light is collected; this effect is neglected here.

We consider the intracavity beam to be made up of two counterpropagating beams. The beam propagating towards the collection aperture center is labeled beam 1 and the other beam 2. We define an (x, y, z) Cartesian coordinate system with unit basis vectors $(\hat{x}, \hat{y}, \hat{z})$ so that the z -axis extends through the center of the aperture, and $z = 0$ is defined to be the position where particles cross the z -axis. For our scattering calculations, we neglect the finite spatial extent of the beams and assume an infinite coherence length. We model the beams as linearly polarized plane waves with equal amplitudes and with parallel polarization in the x -direction. We use the $\exp(-i\omega t)$ convention and represent the electrical fields of beam 1 (propagating in the direction of increasing z) and beam 2 (propagating in the direction of decreasing z) as

$$\mathbf{E}_{inc}(\mathbf{r}, t; 1) = \hat{x} E_{inc} \exp[i(kz - \omega t + \Phi_1)]. \quad (\text{A-1a})$$

and

$$\mathbf{E}_{inc}(\mathbf{r}, t; 2) = \hat{x} E_{inc} \exp[i(-kz - \omega t + \Phi_2)]. \quad (\text{A-1b})$$

The wavelength of the beams in the medium (with index of refraction N) surrounding the particle is λ , and the wavenumber is $k = N\omega/c = 2\pi/\lambda$. We explicitly introduce the beam phases Φ_p to facilitate discussion of laser coherence. The total electrical field is the sum of the fields of the two beams,

$$\mathbf{E}_{inc}(\mathbf{r}, t) = \sum_{p=1,2} \mathbf{E}_{inc}(\mathbf{r}, t; p), \quad (\text{A-2})$$

and the time-averaged energy distribution of this monochromatic field is proportional to

$$\begin{aligned}
\mathbf{E}_{inc}(\mathbf{r},t) \cdot \mathbf{E}_{inc}^*(\mathbf{r},t) &= |\mathbf{E}_{inc}(\mathbf{r},t;1)|^2 + |\mathbf{E}_{inc}(\mathbf{r},t;2)|^2 + 2 \operatorname{Re} [\mathbf{E}_{inc}(\mathbf{r},t;1) \cdot \mathbf{E}_{inc}^*(\mathbf{r},t;2)] \\
&= 2(E_{inc})^2 [1 + \cos(2kz + \Phi_{12})] \\
&= 4(E_{inc})^2 \cos^2(kz + \Phi_{12}),
\end{aligned} \tag{A-3}$$

where $\Phi_{12} \equiv \Phi_1 - \Phi_2$. We see that maxima (i.e., antinodes or bright fringes) occur in the energy distribution when $kz + \Phi_{12} = n\pi$, $n = 0, \pm 1, \pm 2, \pm 3, \dots$, and the distance between the antinodes of this interference fringe pattern is $\delta = \pi/k = \lambda/2$. If the coherence time of the beams (T_c) is longer than the transit time (T_t) required for the particle to pass through the beams, then Φ_{12} is constant and the fringes are fixed in space, but if $T_c < T_t$, then Φ_{12} becomes a function of time, as the fringes change during transit.

The two incident electromagnetic waves scatter from the particle crossing the beams, and our immediate goal is to obtain the scattered wave solutions as functions of the variables and basis vectors of a single coordinate system, which we choose to be the (r, θ, ϕ) spherical system (with unit basis vectors $(\hat{r}, \hat{\theta}, \hat{\phi})$ associated with the (x, y, z) Cartesian system. To accomplish this goal, it is helpful to introduce two other Cartesian systems: (x_1, y_1, z_1) with basis vectors $(\hat{x}_1, \hat{y}_1, \hat{z}_1)$ associated with beam 1, and (x_2, y_2, z_2) with basis vectors $(\hat{x}_2, \hat{y}_2, \hat{z}_2)$ associated with beam 2. The origin of these two systems is the center of the particle, and

$$\begin{aligned}
\hat{x}_1 &= \hat{x}_2 = \hat{x}, \\
\hat{y}_1 &= -\hat{y}_2 = \hat{y}, \\
\hat{z}_1 &= -\hat{z}_2 = \hat{z}.
\end{aligned} \tag{A-4}$$

As the particle crosses the beams, the large spatial dimension of the collection aperture compared to that of the aerosol stream that crosses the beam (about $100 \mu\text{m}$) and particle diameter (a few micrometers) allows us to make the approximations

$$\begin{aligned}
x_1 &= x_2 = x, \\
y_1 &= -y_2 = y, \\
z_1 &= -z_2 = z.
\end{aligned} \tag{A-5}$$

The spherical systems associated with these two Cartesian systems are

$$\begin{aligned}(r, \theta_1, \phi_1) &= (r, \theta, \phi), \\ (r, \theta_2, \phi_2) &= (r, \pi - \theta, -\phi),\end{aligned}\quad (\text{A-6})$$

with unit basis vectors

$$\begin{aligned}(\hat{r}, \hat{\theta}_1, \hat{\phi}_1) &= (\hat{r}, \hat{\theta}, \hat{\phi}), \\ (\hat{r}, \hat{\theta}_2, \hat{\phi}_2) &= (\hat{r}, -\hat{\theta}, -\hat{\phi}).\end{aligned}\quad (\text{A-7})$$

We now write the electrical fields of the two incident waves ($p = 1, 2$) as

$$\mathbf{E}_{inc}(\mathbf{r}, t; p) = \hat{x}_p E_{inc} \exp[i(kz_p - \omega t + \Phi_p)], \quad (\text{A-8})$$

and the far-field scattering solutions as

$$\mathbf{E}_{sca}(\mathbf{r}, t; p) = \mathbf{E}_{sca}(\mathbf{r}; p) \exp[i(-\omega_p t + \Phi_p)], \quad (\text{A-9a})$$

where

$$\mathbf{E}_{sca}(\mathbf{r}; p) = (E_{\theta_p} \hat{\theta}_p + E_{\phi_p} \hat{\phi}_p). \quad (\text{A-9b})$$

The scattered fields can be expressed as functions of amplitude scattering matrices (Bohren and Huffman, 1983) with components S_k ($k = 1$ to 4), and for incident fields polarized in the \hat{x}_p direction,

$$\begin{bmatrix} E_{\theta_p} \\ -E_{\phi_p} \end{bmatrix} = E_{inc} \begin{pmatrix} \exp(ik_p r) \\ -ik_p r \end{pmatrix} \begin{bmatrix} S_2(\mu_p) & S_3(\mu_p) \\ S_4(\mu_p) & S_1(\mu_p) \end{bmatrix} \begin{bmatrix} \cos \phi_p \\ \sin \phi_p \end{bmatrix}, \quad (\text{A-9c})$$

where $\mu_p \equiv \cos \theta_p$ and $k_p = N\omega_p/c$. If the particle is a homogeneous sphere, then $S_3 = S_4 = 0$.

Recalling equations (A-6) and (A-7), we find that

$$\begin{aligned}\mathbf{E}_{sca}(\mathbf{r}; 1) &= E_{\theta_1} \hat{\theta}_1 + E_{\phi_1} \hat{\phi}_1, \\ \mathbf{E}_{sca}(\mathbf{r}; 2) &= -E_{\theta_2} \hat{\theta}_2 - E_{\phi_2} \hat{\phi}_2.\end{aligned}\quad (\text{A-10})$$

If the particle does not pass perpendicular to the beam, then it has a small velocity component parallel to the beam axis, and the frequencies of the two scattered waves are slightly unequal because of small Doppler shifts. An appropriate expression given by Jackson (1975, eq (11.8)) can be rewritten to obtain the frequency of incident beam p in the particle's rest frame (PRF) as

$$(\omega_p)_{PRF} = \omega - k\mathbf{v} \cdot \hat{z}_p, \quad (\text{A-11a})$$

and a second Doppler shift of scattered wave p into the lab system gives the frequency of the far-field scattered wave at a point on the aperture (in direction \hat{r}) as

$$\begin{aligned}\omega_p &= (\omega_p)_{PRF} - k\mathbf{v} \cdot \hat{r}, \\ &= \omega + \Delta\omega_p,\end{aligned}\tag{A-11b}$$

where

$$\Delta\omega_p \equiv -k\mathbf{v} \cdot (\hat{z}_p + \hat{r}),\tag{A-11c}$$

so that the difference between the scattered frequencies at a point on the aperture is

$$\begin{aligned}\omega_{21} &\equiv \omega_2 - \omega_1, \\ &= 2k(\mathbf{v} \cdot \hat{z}), \\ &= 2kv_z.\end{aligned}\tag{A-12}$$

The Doppler shift of each beam is position dependent over the aperture, but the difference in frequencies between the two scattered waves (differential Doppler shift) is not position dependent.

The total electric and magnetic fields at point \mathbf{r} on the aperture at time t are

$$\begin{aligned}\mathbf{E}_{sca}(\mathbf{r}, t) &= \sum_{p=1,2} \mathbf{E}_{sca}(\mathbf{r}, t; p), \\ \mathbf{H}_{sca}(\mathbf{r}, t) &= \sum_{p=1,2} \mathbf{H}_{sca}(\mathbf{r}, t; p).\end{aligned}\tag{A-13}$$

and the instantaneous Poynting vector is

$$\mathbf{S}(\mathbf{r}, t) = \text{Re}[\mathbf{E}_{sca}(\mathbf{r}, t)] \times \text{Re}[\mathbf{H}_{sca}(\mathbf{r}, t)].\tag{A-14}$$

We assume that all radiant power scattered into the aperture solid angle,

$$P_{\Delta\Omega}(t) = \int_{\Delta\Omega} d\Omega r^2 \hat{r} \cdot \mathbf{S}(\mathbf{r}, t),\tag{A-15}$$

is delivered to the sensing element, which produces an electronic signal proportional to this power. We find that

$$\hat{r} \cdot \mathbf{S}(\mathbf{r}, t) = \frac{N}{2\mu c} \text{Re} \sum_{p=1,2} \sum_{q=1,2} [\mathbf{E}_{sca}(\mathbf{r}; p) \cdot \mathbf{E}_{sca}^*(\mathbf{r}; q)] \exp[i(-\omega_{pq}t + \Phi_{pq})],\tag{A-16}$$

where $\omega_{pq} \equiv \omega_p - \omega_q$ and $\Phi_{pq} \equiv \Phi_p - \Phi_q$. The time-averaged irradiance of each incident beam is

$$I_{inc} = \frac{N}{2\mu c} (E_{inc})^2, \quad (\text{A-17})$$

so that

$$P_{\Delta\Omega}(t)/I_{inc} = \text{Re} \sum_{p=1,2} \sum_{q=1,2} W_{pq} \exp[i(\omega_{qp}t + \Phi_{pq})], \quad (\text{A-18a})$$

where

$$W_{pq} \equiv \frac{1}{k_p k_q} \int_{\Delta\Omega} d\Omega(k_p r)(k_q r) \mathbf{E}_{sca}(\mathbf{r}; p) \cdot \mathbf{E}_{sca}^*(\mathbf{r}; q) / (E_{inc})^2. \quad (\text{A-18b})$$

We observe that $W_{pq}^* = W_{qp}$ so that W_{11} and W_{22} are real.

In order to obtain a realistic simulation of the response function, we need to consider the averaging effect of signal processing by the probe sensor electronics. To do this we examine the passage of the particle through the beams from entrance at time $t = 0$ until exit at $t = T_t$. After the particle enters the beams, scattered light begins to reach the sensor, producing a signal that peaks as the particle reaches the maximum irradiance at the z -axis when $t \simeq T_t/2$. The instrument response to a particle passing through the beams is obtained by electronic averaging of the signal generated by the sensor over an interval of time T_e (a characteristic RC time constant of the sensor amplifiers) centered on the occurrence of the peak signal at $t \simeq T_t/2$. We compute the instrument response R by averaging equation (A-18a) over the appropriate interval of time,

$$\begin{aligned} R &= \langle P_{\Delta\Omega}(t)/I_{inc} \rangle \\ &= \frac{1}{T_e} \int_{t=T_t/2-T_e/2}^{t=T_t/2+T_e/2} dt [P_{\Delta\Omega}(t)/I_{inc}], \\ &= \text{Re} \sum_{p=1,2} \sum_{q=1,2} W_{pq} \langle \exp[i(\omega_{qp}t + \Phi_{pq})] \rangle \\ &= W_{11} + W_{22} + 2 \text{Re}[W_{12} \langle \exp[i(\omega_{21}t + \Phi_{12})] \rangle]. \end{aligned} \quad (\text{A-19})$$

Thus the response function consists of three cross-section components: one associated with beam 1, one with beam 2, and an interference term.

A-2 Corrected PAG Response Function

We now derive a new expression of the PAG theory, which is applicable when the particle's trajectory is exactly transverse to the beams (i.e., $\omega_{21} = 0$ and $k_1 = k_2 = k$) at the position of an unmoving bright fringe (antinode) so that $\Phi_{12} = 0$. These assumptions reduce equation (A-19) to

$$R = W_{11} + W_{22} + W_{12} + W_{21} , \quad (\text{A-20})$$

where

$$\begin{aligned} W_{11} &= \frac{\pi}{k^2} \int_{\mu_{\max}}^{\mu_{\min}} d\mu \left[|S_1(\mu)|^2 + |S_2(\mu)|^2 + |S_3(\mu)|^2 + |S_4(\mu)|^2 \right] , \\ W_{22} &= \frac{\pi}{k^2} \int_{\mu_{\max}}^{\mu_{\min}} d\mu \left[|S_1(-\mu)|^2 + |S_2(-\mu)|^2 + |S_3(-\mu)|^2 + |S_4(-\mu)|^2 \right] , \\ W_{12} &= \frac{\pi}{k^2} \int_{\mu_{\max}}^{\mu_{\min}} d\mu \left[S_1(\mu)S_1^*(-\mu) - S_2(\mu)S_2^*(-\mu) + S_3(\mu)S_3^*(-\mu) - S_4(\mu)S_4^*(-\mu) \right] , \\ W_{21} &= \frac{\pi}{k^2} \int_{\mu_{\max}}^{\mu_{\min}} d\mu \left[S_1^*(\mu)S_1(-\mu) - S_2^*(\mu)S_2(-\mu) + S_3^*(\mu)S_3(-\mu) - S_4^*(\mu)S_4(-\mu) \right] ; \end{aligned}$$

and where $\mu_{\min} \equiv \cos \theta_{\min}$ and $\mu_{\max} \equiv \cos \theta_{\max}$. We observe that equation (A-20) can be rewritten as

$$\begin{aligned} R &\simeq \frac{\pi}{k^2} \int_{\mu_{\max}}^{\mu_{\min}} d\mu \left[|S_1(\mu) + S_1(-\mu)|^2 + |S_2(\mu) - S_2(-\mu)|^2 \right. \\ &\quad \left. + |S_3(\mu) + S_3(-\mu)|^2 + |S_4(\mu) - S_4(-\mu)|^2 \right] , \quad (\text{A-21}) \end{aligned}$$

and if the particle is a homogeneous sphere, then the integrands $S_3(\mu) = S_4(\mu) = S_3(-\mu) = S_4(-\mu) = 0$, and we obtain

$$R \simeq \pi k^2 \int_{\mu_{\max}}^{\mu_{\min}} d\mu \left[|S_1(\mu) + S_1(-\mu)|^2 + |S_2(\mu) - S_2(-\mu)|^2 \right] . \quad (\text{A-22})$$

We refer to this result as the corrected PAG equation, because it is a corrected version of the original PAG equation given by equation (3) in the main body of the report.

A-3 New Response Function

To obtain a more realistic response function, we now consider particles crossing the nodes, antinodes, and intermediate regions during transit

through the intracavity beam. If the beam fringes do not change or move during particle transit, then Φ_{12} remains constant, and the interference term in equation (A-19) can be simplified, giving

$$R = W_{11} + W_{22} + 2\{\sin(\omega_{21}T_e/2)/(\omega_{21}T_e/2)\} \operatorname{Re}\{W_{12} \exp[i(\omega_{21}T_t/2 + \Phi_{12})]\}. \quad (\text{A-23})$$

Recalling equation (A-12), we find that $\omega_{21}T_e/2 = 2\pi(v_zT_e/\lambda)$. To estimate the magnitude of this term, we assume the diameter of the aerosol stream that intersects the laser beam to be $100 \mu\text{m}$, and the particle's velocity transverse to the beam to be 10 m/s , so that the transit time across the beam, T_t , is $10 \mu\text{s}$. Also, we assume that the particle's velocity is not exactly transverse to the z -axis but has a component v_z that is, let us say, 2° from the perpendicular direction, so that $(v_z)_{\max} = (10 \text{ m/s}) \tan(2^\circ) = 0.349 \mu\text{m}/\mu\text{s}$. Using $\lambda = 0.6328 \mu\text{m}$ and $T_e = 1.0 \mu\text{s}$, we find $\omega_{21}T_e/2 = 2\pi(0.349)(1.0)/0.6328$ and $\sin(\omega_{21}T_e/2)/(\omega_{21}T_e/2) = -0.092$. Thus this factor causes a 91-percent reduction of the magnitude of the third (interference) term in equation (A-23). This reduction is even more for larger values of $\omega_{21}T_e/2 = \pi(v_zT_e/\delta)$. This last expression of $\omega_{21}T_e/2$ is equal to π times the number of fringes that the particle crosses during the time T_e , so the interference term of equation (A-23) becomes smaller if the particle crosses more fringes.

Having demonstrated that the interference term of equation (A-23) is small for realistic particle trajectories through the beam, we turn our attention to an additional effect that may also reduce the magnitude of this term: that of finite laser coherence time. We examine the hypothetical situation when the particle passes exactly perpendicular through the beam so that $v_z = 0$ and $\omega_{21} = 0$ (i.e., there is no differential Doppler shift). Even though there is no Doppler shift, the fringes are not fixed during particle transit, because the laser changes longitudinal modes (Φ_{12} is not constant, as the coherence time of the laser, $T_c \cong 0.5 \mu\text{s}$, is less than the particle transit time and the electronic averaging time). Thus, Φ_1 and Φ_2 each assume multiple random values during particle transit, and we find that

$$\langle \exp[i(\omega_{21}t + \Phi_{12})] \rangle = \frac{1}{T_e} \int_{t=T_t/2-T_e/2}^{t=T_t/2+T_e/2} dt \exp[i\Phi_{12}(t)] \simeq 0. \quad (\text{A-24})$$

We conclude that the response function that accounts for particles crossing fringes of the intracavity beam and the finite coherence time of the laser can be approximated by

$$\begin{aligned}
R &= W_{11} + W_{22} \\
&= \frac{\pi}{k^2} \int_{\mu_{\max}}^{\mu_{\min}} d\mu \left[|S_1(\mu)|^2 + |S_2(\mu)|^2 + |S_3(\mu)|^2 + |S_4(\mu)|^2 \right. \\
&\quad \left. + |S_1(-\mu)|^2 + |S_2(-\mu)|^2 + |S_3(-\mu)|^2 + |S_4(-\mu)|^2 \right], \quad (\text{A-25})
\end{aligned}$$

where we have used the simplifying approximation that, since particle trajectory velocities are within a few degrees of being perpendicular to the beam, $1/(k_1)^2 \simeq 1/(k_2)^2 \simeq 1/k_1 k_2 \simeq 1/k^2$.

If the particle is a homogeneous sphere, then the integrands $S_3(\mu) = S_4(\mu) = S_3(-\mu) = S_4(-\mu) = 0$, and we obtain the new response function:

$$\begin{aligned}
R &\simeq \frac{\pi}{k^2} \int_{\mu_{\max}}^{\mu_{\min}} d\mu \left[|S_1(\mu)|^2 + |S_2(\mu)|^2 \right. \\
&\quad \left. + |S_1(-\mu)|^2 + |S_2(-\mu)|^2 \right]. \quad (\text{A-26})
\end{aligned}$$

A-4 Response Function for Multiline Lasing

Finally, we consider the instrument response for multiline lasing. If the intracavity beam contains multiple frequencies, then the difference between these frequencies is approximately a factor of 10^6 greater than the differential Doppler frequency considered earlier, and the time-dependent interference terms in the total instantaneous Poynting vector are averaged to zero by the sensor. The result is that the time-averaged instantaneous Poynting vector is equal to the sum of the time-averaged Poynting vectors of the different frequencies, and the instrument's response is

$$\begin{aligned}
R &= \frac{\sum_{\lambda} \langle P_{\Delta\Omega}(t, \lambda) \rangle}{\sum_{\lambda} I_{inc}(\lambda)} \\
&= \frac{\sum_{\lambda} R(\lambda) I_{inc}(\lambda)}{\sum_{\lambda} I_{inc}(\lambda)} \\
&= \sum_{\lambda} R(\lambda) f(\lambda), \quad (\text{A-27a})
\end{aligned}$$

where $f(\lambda)$ is the fraction of the total irradiance,

$$f(\lambda) \equiv I_{inc}(\lambda) / \sum_{\lambda} I_{inc}(\lambda). \quad (\text{A-27b})$$

Thus the multifrequency response is the weighted sum of the response functions (of wavelength λ), each weighted by the irradiance fraction at λ .

Appendix B. Normalization of Measured Response to Theory

The measured responses of the PMS probes are fit to the theoretical response as follows. Measurements of the raw response of a particular probe (in volts), $R^{raw}(r_n)$, where r_n is the polystyrene latex particle radius, are taken from the appropriate journal reference for a total of N particle sizes. We restrict the fit to the polystyrene latex data because these particles have well-characterized size and refractive index. The experimental response of the instrument (in centimeters squared), R_n^{exp} , is then given by

$$R_n^{exp} = GR^{raw}(r_n), \quad (\text{B-1})$$

where G is the gain (in centimeters squared per volt) to be determined by comparison of the experimental response with a theoretical cross section (in centimeters squared). The corresponding theoretical response $R_{sym}(r_n)$ is computed with equations (1), (2), or (3) in the main body of the report.

The approach used here is to determine the gain G by minimizing the absolute value of a function $S(G)$ defined as

$$S(G) \equiv \sum_{n=1}^N ([\log_{10}(R_n^{exp})] - [\log_{10}(R_{sym}(r_n))]) . \quad (\text{B-2})$$

This approach, in which the sum of the difference of the logarithm of response is minimized, weighs all response measurements nearly equally in the fitting procedure.

Acknowledgments

We thank Steven C. Hill for verifying equation (1) and Dennis Garvey for helpful comments.

References

- Allan, R. R., and P. C. Ashdown (1982). A note on the response of Knollenberg aerosol counters, *J. Phys. D: Appl. Phys.* **15**: 59–63.
- Barnard, J. C., and L. C. Harrison (1988). Monotonic responses from monochromatic optical particle counters, *Appl. Opt.* **27**: 584–592.
- Bohren, C. F., and D. R. Huffman (1983). *Absorption and Scattering of Light by Small Particles* (Wiley-Interscience, New York), p 63.
- Colbeck, I., E. J. Hardman, and R. M. Harrison (1989). Optical and dynamical properties of fractal clusters of carbonaceous smoke, *J. Aerosol Sci.* **20**: 765–774.
- Chen, B. T., Y. S. Cheng, and H. C. Yeh (1984). Experimental responses of two optical particle counters, *J. Aerosol Sci.* **15**: 457–464.
- Chylek, P., V. Ramaswamy, R. Cheng, and R. G. Pinnick (1981). Optical properties and mass concentration of carbonaceous smokes, *Appl. Opt.* **20**: 2980–2985.
- Forrest, S. R., and T. A. Witten (1979). Long-range correlations in smoke-particle aggregates, *J. Phys. A: Math. Gen.* **12**: L109–L117.
- Garvey, D. M., and R. G. Pinnick (1983). Response characteristics of the Particle Measuring Systems Active Scattering Aerosol Spectrometer Probe (ASASP-X), *Aerosol Sci. Tech.* **2**: 477–488.
- Gillette, D. A., and T. R. Walker (1977). Characteristics of airborne particles produced by wind erosion of sandy soil, high plains of west Texas, *Soil Sci.* **123**: 97–110.
- Hering, S. V., and P. H. McMurry (1991). Optical counter response to monodisperse atmospheric aerosols, *Atmos. Environ.* **25**: 463–468.
- Hinds, W. C., and G. Kraske (1986). Performance of PMS model LAS-X optical particle counter, *J. Aerosol Sci.* **17**: 67–72.
- Jackson, J. D. (1975). *Classical Electrodynamics*, 2nd ed. (Wiley, New York), p 510.

- Jeung, I. S. (1990). Response characteristics of the Knollenberg active scattering aerosol spectrometer to light-absorbing aerosols, *Opt. Eng.* **29**: 247–252.
- Kim, Y. J. (1995). Response of the active scattering aerosol spectrometer probe (ASASP-100X) to particles of different chemical composition, *Aerosol Sci. Tech.* **22**: 33–42.
- Kim, Y. J., and J. F. Boatman (1990). Size calibration corrections for the active scattering aerosol spectrometer probe (ASASP-100X), *Aerosol Sci. Tech.* **12**: 665–672.
- Knollenberg, R. G. (1976). The use of low power lasers in particle size spectrometry, *SPIE*. **92**: 137–162.
- Knollenberg, R. G. (1989). The measurement of latex particle sizes using scattering ratios in the Rayleigh-scattering size range, *J. Aerosol Sci.* **20**: 331–345.
- Knollenberg, R. G., and D. L. Veal (1992). Optical particle monitors, counters, and spectrometers: Performance characterization, comparison, and use, *J. Inst. Environ. Sci.* **35**: 64–81.
- Liu, B.Y.H., W. W. Szymanski, and K. H. Ahn (1985). On aerosol size distribution measurement by laser and white light optical particle counters, *J. Environ. Sci.* **28**: 19–24.
- Liu, P.S.K., W. R. Leitch, J. W. Strapp, and M. A. Wasey. (1992). Response of Particle Measuring Systems airborne ASASP and PCASP to NaCl and latex particles, *Aerosol Sci. Tech.* **16**: 83–95.
- Ngo, D., G. Videen, and P. Chylek (1996). A FORTRAN code for the scattering of EM waves by a sphere with a nonconcentric spherical inclusion. *Computer Phys. Commun.* **1077**: 94–112.
- Pinnick, R. G., and H. J. Auvermann (1979). Response characteristics of Knollenberg light-scattering aerosol counters, *J. Aerosol Sci.* **10**: 55–74.
- Pinnick, R. G., G. Fernandez, B. D. Hinds, C. W. Bruce, R. W. Schaefer, and J. D. Pendleton (1985). Dust generated by vehicular traffic on unpaved roadways: Sizes and infrared extinction characteristics, *Aerosol Sci. Tech.* **4**: 99–121.
- Pinnick, R. G., and J. M. Rosen (1979). Response of Knollenberg light-scattering counters to non-spherical doublet polystyrene latex aerosols, *J. Aerosol Sci.* **10**: 533–538.

- Prospero, J. M., R. J. Charlson, V. Mohnen, R. Jaenicke, A. C. Delany, J. Moyers, W. Zoller, and K. Rahn (1983). The atmospheric aerosol system: An overview, *Rev. Geophys. Space Phys.* **21**: 1607–1629.
- Pueschel, V. R., V. R. Overbeck, K. G. Snetsinger, P. B. Russell, G. V. Ferry, J. C. Wilson, J. M. Livingston, S. Verma, and W. Fong (1990). Calibration correction of an active scattering spectrometer probe to account for refractive index of stratospheric aerosols: Comparison of results with inertial impaction, *Aerosol Sci. Tech.* **12**: 992–1002.
- Rietmeijer, F.J.M., and J. Janeczek (1997). An analytical electron microscope study of airborne industrial particles in Sosnowiec, Poland, *Atmos. Environ.* **31**: 1941–1951.
- Schuster, B. G., and R. Knollenberg (1972). Detection and sizing of small particles in an open cavity gas laser, *Appl. Opt.* **11**: 1515–1520.
- Sheridan, P. J., and I. H. Musselman (1985). Characterization of aircraft-collected particles present in the Arctic aerosol; Alaskan Arctic, spring 1983, *Atmos. Environ.* **19**: 2159–2166.
- Sheridan, P. J. (1989a). Analytical electron microscope studies of size-segregated particles collected during AGASP-II, flights 201–203, *J. Atmos. Chem.* **9**: 267–282.
- Sheridan, P. J. (1989b). Characterization of size segregated particles collected over Alaska and the Canadian high arctic, AGASP-II flights 204–206, *Atmos. Environ.* **11**: 2371–2386.
- Sheridan, P. J., R. C. Schnell, J. D. Kah, J. F. Boatman, and D. M. Garvey (1993). Microanalysis of the aerosol collected over south-central New Mexico during the ALIVE field experiment, May–Dec 1989, *Atmos. Environ.* **8**: 1169–1183.
- Soderholm, S. C., and G. C. Salzman (1984). Laser spectrometer: Theory and practice, *Aerosols* (B.Y.H. Liu, D.Y.H. Pui, and H. J. Fissan, eds.). Elsevier Science Publishing Co., Amsterdam, pp 11–14.
- Szymanski, W. W., and B.Y.H. Liu (1986). On the sizing accuracy of laser optical particle counters, *Part. Charact.* **3**: 1–7.
- Videen, G., D. Ngo, P. Chylek, and R. G. Pinnick (1995). Light scattering from a sphere with an irregular inclusion, *J. Opt. Soc. Am. A* **12**: 922–928.
- Yamada, Y., K. Miyamoto, and A. Koizumi (1986). Size measurements of latex particles by laser aerosol spectrometer, *Aerosol Sci. Tech.* **5**: 377–384.

Distribution

Admnstr
Defns Techl Info Ctr
Attn DTIC-OCF
8725 John J Kingman Rd Ste 0944
FT Belvoir VA 22060-6218

Central Intllgnc Agency Dir DB Standard
Attn OSS/KPG/DHRT
1E61 OHB
Washington DC 20505

Chairman Joint Chiefs of Staff
Attn J5 R&D Div
Washington DC 20301

Dir of Defns Rsrch & Engrg
Attn DD TWP
Attn Engrg
Washington DC 20301

Ofc of the Secy of Defns
Attn ODDRE (R&AT)
The Pentagon
Washington DC 20301-3080

Ofc of the Secy of Defns
Attn OUSD(A&T)/ODDR&E(R) R J Trew
3080 Defense Pentagon
Washington DC 20301-7100

Commanding Officer
Attn NMCB23
6205 Stuart Rd Ste 101
FT Belvoir VA 22060-5275

CECOM
Attn PM GPS COL S Young
FT Monmouth NJ 07703

Dir of Chem & Nuc Ops DA DCSOPS
Attn Techl Lib
Washington DC 20301

US Army Engrg Div
Attn HNDED FD
PO Box 1500
Huntsville AL 35807

US Army ERDEC
Attn SCBRD-RTE I Sindoni
Attn SCBRD-RTE J Embury

US Army ERDEC (cont'd)
Attn SCBRD-RTE M Milham
Attn SCBRD-RTE S Christesen
Aberdeen Proving Ground MD 21005-5423

US Army Mis & Spc Intllgnc Ctr
Attn AIAMS YDL
Redstone Arsenal AL 35898-5500

US Army NGIC
Attn Rsrch & Data Branch
220 7th Stret NE
Charlottesville VA 22901-5396

US Army Nuc & Cheml Agency
7150 Heller Loop Ste 101
Springfield VA 22150-3198

US Army Strtgc Defns Cmnd
Attn CSSD H MPL Techl Lib
PO Box 1500
Huntsville AL 35807

US Military Academy
Mathematical Sci Ctr of Excellence
Attn MDN-A LTC M D Phillips
Dept of Mathematical Sci Thayer Hall
West Point NY 10996-1786

USAF Armstrong Laboratory Edgewood
Rsrch Dev & Engrg Ctr
Attn AMSCB-AL B Bronk
Attn SCBRD-RTE E Stuebing
Attn SCBRD-RTE R Doherty
Aberdeen Proving Ground MD 21010

Chief of Nav OPS Dept of the Navy
Attn OP 03EG
Washington DC 20350

Nav Surface Warfare Ctr
Attn Code B07 J Pennella
17320 Dahlgren Rd Bldg 1470 Rm 1101
Dahlgren VA 22448-5100

U.S. Air Force Tech Appl Ctr
Attn Hq AFTAC/TCC
Attn S Gotoff
1030 South Highway A1A
Patrick AFB FL 32925-3002

Distribution (cont'd)

DARPA
Attn S Welby
Attn Techn Lib
3701 N Fairfax Dr
Arlington VA 22203-1714

US Dept of Energy
Attn KK 22 K Sisson
Attn Techn Lib
Washington DC 20585

Univ of Cincinnati
Dept of Environ Health Aerosol Rsrch Lab
Attn S A Grinshpun
PO Box 670056
Cincinnati OH 45267-0056

Univ of Kentucky
Dept of Chemical Engineering
Attn A K Ray
163 Anderson Hall
Lexington KY 40506-0046

Univ of Wyoming
Dept of Physics & Astronomy
Attn J M Rosen
Laramie WY 82071

Yale Univ
Dept of Applied Physics & Ctr for Laser
Diagnostics
Attn R Chang
New Haven CT 06520-8284

Hicks & Associates Inc
Attn G Singley III
1710 Goodrich Dr Ste 1300
McLean VA 22102

MicroTherm LLC
Attn W Dick
748 Harding Street NE
Minneapolis MN 55413

Particle Measuring Systems Inc
Attn L Fabiny Research Scientist
5475 Airport Blvd
Boulder CO 80301

US Army Rsrch Ofc
Attn AMSRL-RO-EN B Mann
PO Box 12211
Research Triangle Park NC 27709-2211

US Army Rsrch Lab
Attn AMSRL-DD J M Miller
Attn AMSRL-CI-AI-A Mail & Records Mgmt
Attn AMSRL-CI-AP Techn Pub (3 copies)
Attn AMSRL-CI-LL Techn Lib (3 copies)
Attn AMSRL-IS J D Gantt
Attn AMSRL-IS-EE G Videen (20 copies)
Attn AMSRL-IS-EE S Niles
Attn AMSRL-IS-EM D Garvey
Attn AMSRL-IS-EM J D Pendleton
(20 copies)
Attn AMSRL-IS-EM R Pinnick (30 copies)
Attn AMSRL-IS-M S Hill
Adelphi MD 20783-1197

REPORT DOCUMENTATION PAGE			<i>Form Approved OMB No. 0704-0188</i>	
Public reporting burden for this collection of information is estimated to average 1 hour per response, including the time for reviewing instructions, searching existing data sources, gathering and maintaining the data needed, and completing and reviewing the collection of information. Send comments regarding this burden estimate or any other aspect of this collection of information, including suggestions for reducing this burden, to Washington Headquarters Services, Directorate for Information Operations and Reports, 1215 Jefferson Davis Highway, Suite 1204, Arlington, VA 22202-4302, and to the Office of Management and Budget, Paperwork Reduction Project (0704-0188), Washington, DC 20503.				
1. AGENCY USE ONLY <i>(Leave blank)</i>		2. REPORT DATE March 2000	3. REPORT TYPE AND DATES COVERED Summary, June–December 1998	
4. TITLE AND SUBTITLE Response Characteristics of Active Scattering Aerosol Spectrometer Probes Made by Particle Measuring Systems			5. FUNDING NUMBERS DA PR: B53A PE: 61102A	
6. AUTHOR(S) Ronald G. Pinnick, J. David Pendleton, and Gordon Videen				
7. PERFORMING ORGANIZATION NAME(S) AND ADDRESS(ES) U.S. Army Research Laboratory Attn: AMSRL-IS-EM email: rpinnick@arl.mil 2800 Powder Mill Road Adelphi, MD 20783-1197			8. PERFORMING ORGANIZATION REPORT NUMBER ARL-TR-1973	
9. SPONSORING/MONITORING AGENCY NAME(S) AND ADDRESS(ES) U.S. Army Research Laboratory 2800 Powder Mill Road Adelphi, MD 20783-1197			10. SPONSORING/MONITORING AGENCY REPORT NUMBER	
11. SUPPLEMENTARY NOTES ARL PR: 9FEJ71 AMS code: 61110253A11				
12a. DISTRIBUTION/AVAILABILITY STATEMENT Approved for public release; distribution unlimited.			12b. DISTRIBUTION CODE	
13. ABSTRACT <i>(Maximum 200 words)</i> Predictions are reported of the size response of various light-scattering aerosol counters manufactured by Particle Measuring Systems. Models considered are those that exploit the high intensity of light available within the cavity of a HeNe gas laser (generically referred to by the manufacturer as "active scattering aerosol spectrometer probes"). The new response function properly averages over particle trajectories through nodes, antinodes, and intermediate regions of the intracavity laser beam. Our studies address probes having two basic scattering geometries: those that collect light scattered over a relatively narrow solid angle (subtending angles between 4° and 22° from the laser beam axis) and those that collect light over a rather large solid angle (between 35° and 120°). The new response function predicts smoother dependence on particle size than the previous response function of Pinnick and Auvermann (1979, J. Aerosol Sci. 10: 55–74) and is in better agreement with measurement. Response calculations for common atmospheric aerosol (water, sulfuric acid, ammonium sulfate, and black carbon) reveal the considerable sensitivity of the response to particle dielectric properties. Comparison of response calculations with the manufacturer's calibration reveals conditions for which the manufacturer's calibration is most appropriate, and the potential for errors (as much as a factor of two in sizing) when it is blindly applied. These results should help the user of these instruments to more realistically interpret size distribution measurements.				
14. SUBJECT TERMS Aerosol counter			15. NUMBER OF PAGES 50	
			16. PRICE CODE	
17. SECURITY CLASSIFICATION OF REPORT Unclassified		18. SECURITY CLASSIFICATION OF THIS PAGE Unclassified	19. SECURITY CLASSIFICATION OF ABSTRACT Unclassified	20. LIMITATION OF ABSTRACT UL